AIChE WILEY InterScience DISCOVER SOMETHING GREAT

$SrCe_{0.95}Yb_{0.05}O_{3-\alpha}$ Hollow-Fiber Membrane and Its Property in Proton Conduction

Yutie Liu, Xiaoyao Tan, and K. Li
Dept. of Chemical Engineering, Imperial College London, University of London, South Kensington, London SW7 2AZ, U.K.

DOI 10.1002/aic.10738
Published online December 1, 2005 in Wiley InterScience (www.interscience.wiley.com).

$SrCe_{0.95}Yb_{0.05}O_{3-\alpha}$ (SCYb) hollow-fiber membranes have been prepared by an immersion-induced phase-inversion/sintering method where polyethersulfone (PESf) is used as a binder, N-methyl-2-pyrrollidone (NMP) as solvent, and polyvinylpyrrolidone (PVP, K16–18) as an additive, respectively. By a programmed sintering process, the hollow-fiber precursor prepared from the phase-inversion technique has been successfully sintered into a dense membrane. A hollow-fiber membrane module has also been fabricated and the hydrogen permeation (proton conduction) properties of the developed SCYb hollow-fiber membranes have been studied under different operating conditions with respect to temperature and hydrogen/oxygen feed concentration. Comparison between experimental data and theoretical results indicates that the surface exchange reactions may contribute some resistances to hydrogen permeation. With the length of the fiber and operating conditions used in this study, the flow patterns show no noticeable effect on the total hydrogen permeation flux. © 2005 American Institute of Chemical Engineers *AIChE J,* 52: 1577–1585, 2006

Keywords: $SrCe_{0.95}Yb_{0.05}O_{3-\alpha}$; perovskite; hollow-fiber membrane; hydrogen permeation.

Introduction

High-temperature proton/hole conductors based on solid oxides with perovskite structures, such as $SrCe_{0.95}Yb_{0.05}O_{3-\alpha}$ (SCYb), have attracted considerable interest because of their potential applications in the chemical and electrochemical industries.[1-3] However, it is also recognized that considerable efforts have to be devoted to improve their proton conductivity (or hydrogen permeation flux when imposed with an asymmetric environment) before they can be useful in many practical applications. Recently, some progress has been achieved in preparing the dense ceramic membranes with ideal hydrogen permeation fluxes. Hamakawa et al.[4] prepared a thin SCYb film (up to 2 μm) on a porous substrate by spin coating colloidal suspensions of the SCYb powders, and the hydrogen permeation flux as high as 1.2×10^{-3} mol cm^{-2} min^{-1} was achieved at 950 K. In addition, a phase-inversion/sintering technique has been developed in preparing hollow-fiber ceramic membranes with asymmetric structures,[5-7] which show several advantages over conventional membranes. Compared to disk-shaped membranes, hollow-fiber membranes can provide a much larger effective membrane area per unit volume for hydrogen permeation. Also, by adopting long hollow fibers and keeping the two sealing ends away from the high-temperature zone, problems of high-temperature sealing can be avoided. Furthermore, because of the asymmetric structure (that is, a thin separating dense layer integrated on a porous substrate of the same material), the membrane's resistance to hydrogen permeation (or proton conduction) is substantially reduced compared to that of symmetric membranes prepared by conventional methods.

In this work, $SrCe_{0.95}Yb_{0.05}O_{3-\alpha}$ (SCYb) hollow-fiber dense membranes have been successfully prepared by an immersion-induced phase-inversion/sintering technique. The hydrogen permeation (or proton conduction) properties of the resulting SCYb hollow-fiber membranes have also been investigated both experimentally and theoretically.

Correspondence concerning this article should be addressed to K. Li at Kang.Li@Imperial.ac.uk.

Table 1. Spinning Conditions of the SCYb Hollow-Fiber Membrane Precursors

Parameter	Value
Compositions of the starting solution (wt %)	
SCYb powder	69
PESf	7.0
PVP (K90)	0.7
NMP	23.3
Internal coagulant	DI water
External coagulant	Tap water
Spinneret dimension (mm)	
ID/OD	1.2/3.0
Temperature (°C)	22
Air gap (mm)	30

Experimental

Materials

Commercially available $SrCe_{0.95}Yb_{0.05}O_{2.975}$ (SCYb) powders (supplied by Praxair Surface Technologies, Indianapolis, IN) were used as the membrane material. Polyethersulfone (PESf, Radel A-300; Ameco Performance, Greenville, SC), *N*-methyl-2-pyrrollidone (NMP, >99%, Acros Organics, Morris Plains, NJ), and polyvinylpyrrolidone (PVP K90, Acros) were used as binder, solvent, and additive, respectively. Deionized water and tap water were used as the internal and external coagulants, respectively.

Preparation of SCYb hollow-fiber membranes

The immersion-induced phase-inversion/sintering technique was used in preparing the SCYb hollow-fiber membranes. The detailed procedures are described elsewhere.[6] A spinneret with orifice-diameter/inner-diameter ratio of 3.0/1.2 mm was used to obtain the hollow-fiber precursors. The parameters for preparation of the SCYb hollow-fiber precursors are summarized in Table 1.

Sintering of the hollow-fiber membranes was carried out in a high-temperature tubular furnace (STF16/450, Carbolite, Watertown, WI) where the SCYb hollow-fiber precursors were placed and sintered at 1200°C for 16 h and further sintered at 1350–1550°C for another 4 h to form the hollow-fiber membrane product. The heating and cooling rates were both controlled at 5°C/min.

Characterization methods

Structures of the prepared hollow-fiber membranes were visually observed using a scanning electron microscope (SEM; JSM-5610LV, JEOL, Tokyo, Japan). To maintain the original cross-sectional fracture of the hollow-fiber precursor (it is very soft at ambient temperature), it was immersed in liquid nitrogen for about 5–10 min, where the membrane precursor was frozen and then slowly flexed into a short sample with tweezers. For the sintered membranes, the cross-sectional fracture was obtained by directly snapping the fiber. These membrane samples were then positioned on a metal holder and sputter coated with gold under vacuum. SEM photomicrographs of both surface and cross section of the hollow-fiber membranes were taken at various magnifications.

The gastight property of the prepared hollow-fiber membranes was measured using an in-house–developed gas permeation apparatus.[8] Nitrogen was used as the test gas. The initial amount of the test gas in the cylinder was set at 356 kPa and the pressure change was then recorded continuously. The nitrogen permeance through the membrane defects was calculated based on the pressure change in the test cylinder as a function of time. In general, the hollow fiber with a measured permeance of 10,000 times less than the actual permeace of a permeating gas measured at high temperature is considered to be gastight.

The mechanical strength of the hollow fiber was measured through a bending test performed using an Intron Model 4466 provided with a load cell for 1 kN. The hollow-fiber samples were fixed in the sample holder with a spec gauge length of 15 mm. The crosshead speed was set at 0.02 cm/min. The load needed to break the hollow fiber was recorded for each sample with which the bending strength σ_F is calculated using the following equation:

$$\sigma_F = \frac{8F_m L_h D_o}{\pi(D_o^4 - D_i^4)} \tag{1}$$

where F_m is the force at which fracture takes place and L_h, D_o, and D_i are the length (15 mm), outer diameter (OD), and inner diameter (ID) of the hollow fiber, respectively. Final results were taken from the average value of four samples for each membrane.

X-ray diffraction (XRD) analysis was carried out to determine the crystalline structure of the SCYb using a PW1710 X-ray diffractometer with Cu–K_α radiation on the membrane material (SCYb powders), the fresh hollow-fiber membrane [after sintering but before hydrogen (proton) permeation experiments] and on the used membranes taken from the middle section of the hollow fibers after performing the hydrogen permeation. Both the fresh and used membranes were XRD-analyzed on the outer surfaces of snapped fibers. Therefore, the XRD analysis of used membranes reveals the structure only at the outer surface after hydrogen permeation. A continuous scan mode was used to collect 2θ data from 15 to 75° with a 0.04 sampling pitch and a 2.4°/min scan rate. The generator tension and generator current were 40 kV and 40 mA, respectively.

Measurement of hydrogen permeation

The hydrogen permeation (or proton conduction) properties of the resulting SCYb hollow-fiber membranes were studied using a membrane module where a gastight SCYb hollow fiber with 30 cm in length was assembled. Figure 1 illustrates the experimental setup. The membrane module was placed in a tubular furnace (MTF 10/25/130, Carbolite) with a constant temperature zone of only 4.0 cm. Therefore, the two sealing joints were kept away from the furnace tube. A short, soft silicone rubber tube was used to offset the thermal expansion mismatch of the hollow-fiber membrane and the module shell at high temperatures.

In the measurements, the mixture of hydrogen and argon was fed into the shell side, whereas air was introduced into the lumen side of the module. The gas flow rates were controlled and measured using mass flow controllers (Smart Mass Flow meter with Readout & Control Electronics, Model 0152, Brooks Instrument). The temperature was measured with a type C thermocouple combined with a thermometer supplied by

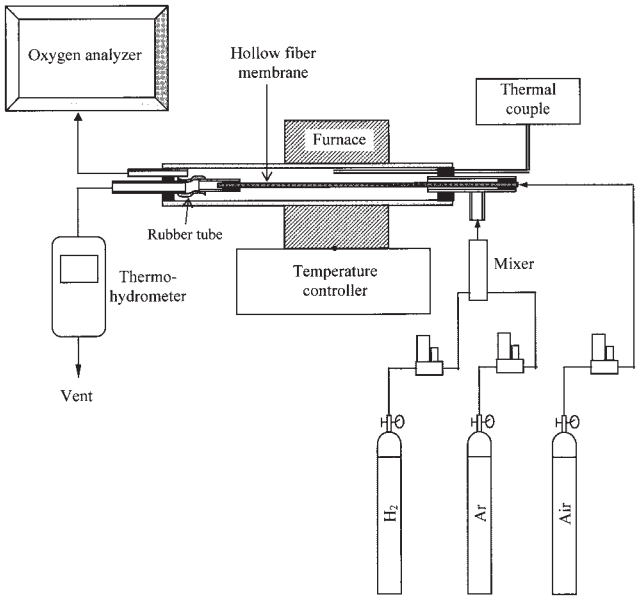

Figure 1. Experimental setup for hydrogen (proton) permeation.

Omega Engineering Inc. Typical feed flow rates were 60 cm^3 (STP)/min for air and 136 cm^3 (STP)/min for hydrogen, respectively. The operating temperatures, listed in Table 2, were operated between 973 and 1173 K. Oxygen concentrations were measured with an oxygen meter (Oxygen Analyzer 572, Servomex). The concentrations of water vapor in gas streams were measured online in terms of relative humidity (RH) using a thermohydrometer supplied by Omega (Model RH82). Obviously, the permeation fluxes of hydrogen and oxygen through the membrane can be reflected by the formation rates of water vapor in the air stream and in the hydrogen stream, respectively. Every experiment was repeated three times. An average value was obtained and the difference was $<5\%$.

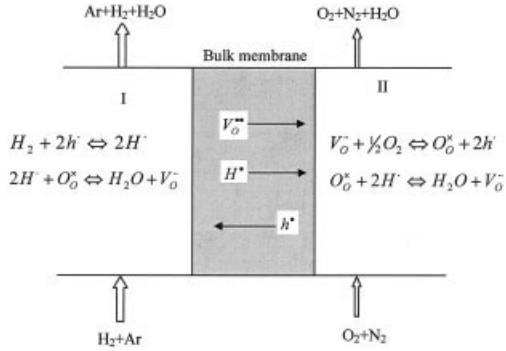

Figure 2. Mechanism of ion permeation in the SCYb membrane.

Theory and Model Development

It is known that SCYb is mainly a mixed proton-hole conductor[9] (its oxygen conduction becomes noticeable only at temperatures $>$ 1400 K) where the mobile charged defects at elevated temperatures include oxygen vacancy $V_o^{\bullet\bullet}$, proton $H^{\bullet}$, and electron hole $h^{\bullet}$.[10,11] When a SCYb membrane is exposed to an asymmetric gas environment, as shown in Figure 2, the charged defects are transferred from one side to the other under the electrochemical potential gradients. The transfer fluxes of the charged defects are described by a group of ordinary differential equations,[9] given in the Appendix A.

Establishment of the modeling equations is based on the membrane module consisting of n SCYb hollow fibers with the length of L, housed in a ceramic tube. The mixture of hydrogen and argon is introduced into the shell side of the module under the atmospheric pressure, whereas air flows through the fiber lumen either cocurrently or countercurrently. The flow pattern in one SCYb hollow fiber is shown in Figure 3.

The following assumptions are adopted to formulate the mathematical model:

(1) The membrane module is isothermally operated at steady state.

Table 2. Characteristic Parameters of the SCYb Hollow-Fiber Membrane and Diffusional/Equilibrium Parameters Used for Calculations

Kinetic Parameter	Value	Reference
Concentration of ytterbium	$[Yb'_{Ce}] = 1.06 \times 10^{-3}$, mol cm^{-3}	13
Diffusivity of proton	$D_p = 0.122 \exp(-7851/T)$, $cm^2\ s^{-1}$	14
Diffusivity of oxygen vacancy	$D_V = 24.24 \exp(-23467/T)$, $cm^2\ s^{-1}$	15
Diffusivity of electron hole	$D_h = 49.38 \exp(12588.7/T)$, $cm^2\ s^{-1}$	16
Equilibrium constant of reaction (1)	$K_1 = 3.24 \times 10^{-8}\exp(1371.3/T)$, mol $atm^{-0.5}\ cm^{-3}$	16
Equilibrium constant of reaction (2)	$K_2 = 1.77 \times 10^{-10}\exp(21911/T)$, mol $atm^{-1}\ cm^{-3}$	16
Equilibrium constant of water formation reaction	$K_w = 1.188 \times 10^{-3}\exp(29709/T)$, $atm^{-1/2}$	17
Fiber Characteristics and Experimental Conditions		
Number of hollow fibers	$n = 1$	
OD of the hollow fiber	$d_o = 0.145$, cm	
ID of the hollow fiber	$d_i = 0.065$, cm	
Effective length of hollow fiber	$L = 4$, cm	
Operating temperature	$T = 973$–1173 K	
Feed concentration of hydrogen	$y_{H_2} = 0.035$–0.36	
Feed concentration of oxygen	$y_s = 0.017$–0.21	
Feed flow rate of air stream	$Q_s = 60$, $cm^3\ min^{-1}$ (STP)	
Feed flow rate of hydrogen stream	$Q_f = 136$, $cm^3\ min^{-1}$ (STP)	
Vapor concentrations in feed streams	$y_{H_2O} = 4 \times 10^{-4}$	

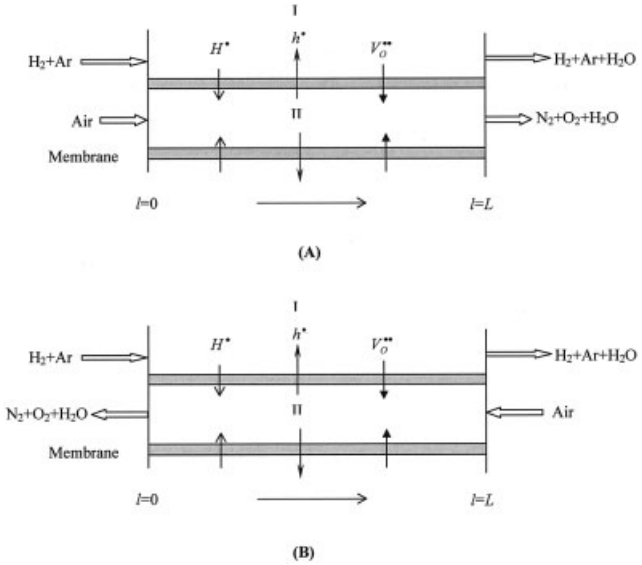

Figure 3. Flow pattern in the SCYb hollow-fiber membrane module.

(A) Cocurrent flow; (B) countercurrent flow.

(2) The transfer of defects in the membrane is the controlling step and the surface reactions are in equilibrium.

(3) The transfer of defects in the axial direction within the membrane is negligible because of the high ratio of the fiber length and the membrane wall thickness.

(4) The mass transfer resistance between gas and the membrane surfaces, either on the shell or lumen side, is negligible.

(5) The ideal gas law may be used to describe the gas behavior of both the single component and the gas mixture.

(6) Plug flow is applied to both the shell and lumen gas streams.

(7) The pressure drop in either lumen or shell side is negligible.

On the shell (hydrogen) side, the mass conservation equations are given by

$$\frac{dN^{I}_{H_2O}}{dl} = 2n\pi R_m \cdot J_V \tag{2a}$$

$$\frac{dN_{H_2}}{dl} = 2n\pi R_m \frac{1}{2} J_h \tag{2b}$$

where N represents the molar flow rates in each component (mol/s). R_m is the average membrane radius, where $R_m = (R_o - R_{in})/[\ln(R_o/R_{in})]$, in which R_o and R_{in} are, respectively, the outer and the inner radius of the hollow fiber. J_V and J_h are the transfer flux of vacancy and hole, respectively.

On the lumen (air) side, the mass conservation equations are given by

For the Cocurrent Flow

$$\frac{dN^{II}_{H_2O}}{dl} = 2n\pi R_m \frac{1}{2} J_p \tag{3a}$$

$$\frac{dN_{O_2}}{dl} = 2n\pi R_m \frac{1}{4} J_h \tag{3b}$$

For the Countercurrent Flow

$$\frac{dN^{II}_{H_2O}}{dl} = -2n\pi R_m \frac{1}{2} J_p \tag{3c}$$

$$\frac{dN_{O_2}}{dl} = -2n\pi R_m \frac{1}{4} J_p \tag{3d}$$

With the following boundary conditions:

For the Cocurrent Flow

$$l = 0 \qquad [N^{I}_{H_2O}, N_{H_2}, N^{II}_{H_2O}, N_{O_2}] = \left[\frac{p_s V_s y_{H_2O,s}}{RT}, \frac{p_s V_s y_{H_2,s}}{RT}, \frac{p_l V_l y_{H_2O,l}}{RT}, \frac{p_l V_l y_{O_2,l}}{RT}\right] \tag{4a}$$

For the Countercurrent Flow

$$l = 0 \qquad [N^{I}_{H_2O}, N_{H_2}] = \left[\frac{p_s V_s y_{H_2O,s}}{RT}, \frac{p_s V_s y_{H_2,s}}{RT}\right] \tag{4b}$$

$$l = L \qquad [N^{II}_{H_2O}, N_{O_2}] = \left[\frac{p_l V_l y_{H_2O,l}}{RT}, \frac{p_l V_l y_{O_2,l}}{RT}\right] \tag{4c}$$

where p_s and p_l are the operating pressures in the shell side and the lumen side, respectively; V_s and V_l are the volumetric feed flow rates of hydrogen mixture and of the air stream, respectively; y is the molar fraction of each component in the gas feed; and L is the effective length of the membranes for permeation.

Although the SCYb membrane conducts proton and oxygen vacancy, the permeation flux of either proton or oxygen vacancy cannot be measured directly from the experiment, but instead, can be calculated only from the formation rate of water on the oxygen side and on the hydrogen side, respectively, as shown Figure 2:

$$J_p = \frac{2}{A_m}(N^{II}_{H_2O,l=L} - N^{II}_{H_2O,l=0}) \tag{5a}$$

$$J_V = \frac{N^{I}_{H_2O,l=L} - N^{I}_{H_2O,l=0}}{A_m} \tag{5b}$$

where A_m is the effective membrane area for permeation, $A_m = 2n\pi R_m L$.

Solution method

As described above, the governing equations for the hollow-fiber membrane module are a group of implicit ordinary differential equations and can be solved numerically only by the Runge–Kutta method. To solve the governing equations for the countercurrent flow pattern, the shooting method has been applied. MATLAB® software (The MathWorks, Natick, MA)

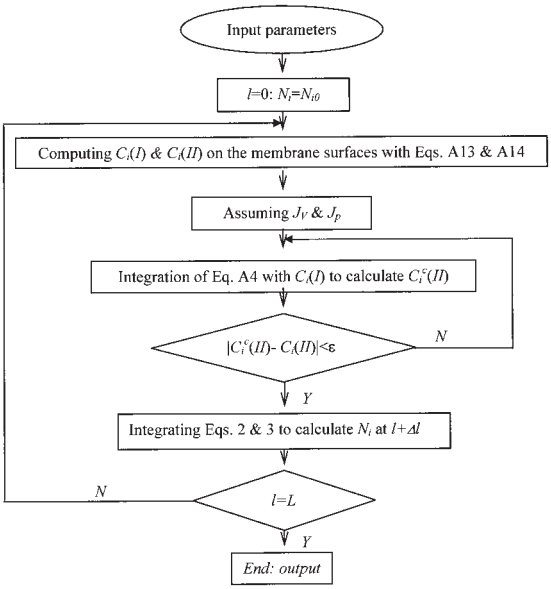

Figure 4. Algorithm of the numerical solution.

was used in this study for the calculations. The numerical solution algorithm is given in Figure 4.

Results and Discussion

Morphology of the SCYb hollow-fiber membranes

Figure 5 exhibits the microstructures of the SCYb hollow-fiber precursors (before sintering) and of the hollow-fiber membrane products, which were sintered following a programmed sintering procedure.[12] The OD/ID of the hollow-fiber precursor was 1.85/0.80 mm, as measured from Figure 5a. After sintering, the corresponding OD/ID of the fiber product was reduced to 1.45/0.65 mm, respectively (Figure 5A). Such a considerable shrinkage resulted from the removal of organic binder and the rearrangement of the SCYb particles in the fibers as well. However, for a certain type of ceramic membranes, the extent of shrinkage is a function of multiple factors, such as the particle size and its size distribution, the content of the polymer binder in the precursor, and the sintering temperature.[12]

Figures 5a and 5b also illustrate the morphologies of the hollow-fiber precursor. It can be seen that a fingerlike structure is formed beneath both the inner and outer skin layers of the hollow-fiber precursor, but a spongelike layer occurs at the center of the fiber precursor. The formation of this type of structure can be attributed not only to the rapid precipitation that occurs at both the inner and outer walls close to coagulants, resulting in finger pores beneath the skin layers, but also to the slow precipitation at the center of the fiber, giving it a spongelike structure, which is also shown in Figure 5c under high magnification. Figure 5d shows the outer surface of the hollow-fiber precursor, from which it can be seen that the SCYb particles are well dispersed and sparsely connected to each other by the polymer binder.

After sintering, the original structure can still be observed, as shown in Figures 5A and 5B. However, the quantity and the size of the fingerlike pores have been substantially reduced after the sintering process. Figure 5D shows the membrane's outer surface. It can be seen that the surface is completely densified and the SCYb particles are closely connected to each other with clear boundaries. Further, most particles are >1 μm, instead of the original size of around 1.0 μm, indicating that particle growth has occurred during the sintering process, where the small discrete particles are combined into larger ones by the sintering. It is interesting to note that all the SCYb particles at the central layer of the fiber have also been densified and seem to be integrated into a dense layer, as shown in Figure 5C.

A gas permeation test was performed to confirm that the prepared SCYb hollow-fiber membrane is gastight when it is sintered at 1450–1500°C. The initial pressure in the test cylinder (upstream pressure) was set at 356 kPa, whereas the other side was connected to the atmosphere. After 24 h, the pressure in the test cylinder was changed from 356 to 342 kPa, from which the gas permeance of the fiber was calculated to be 1.66×10^{-15} mol/(cm^2 Pa·s^{-1}). This permeance value is a few orders of magnitudes smaller than the actual proton permeance (see results in the following section). It should also be noted that the decrease of pressure in the test cylinder may have resulted from not only the gas permeation through the mem-

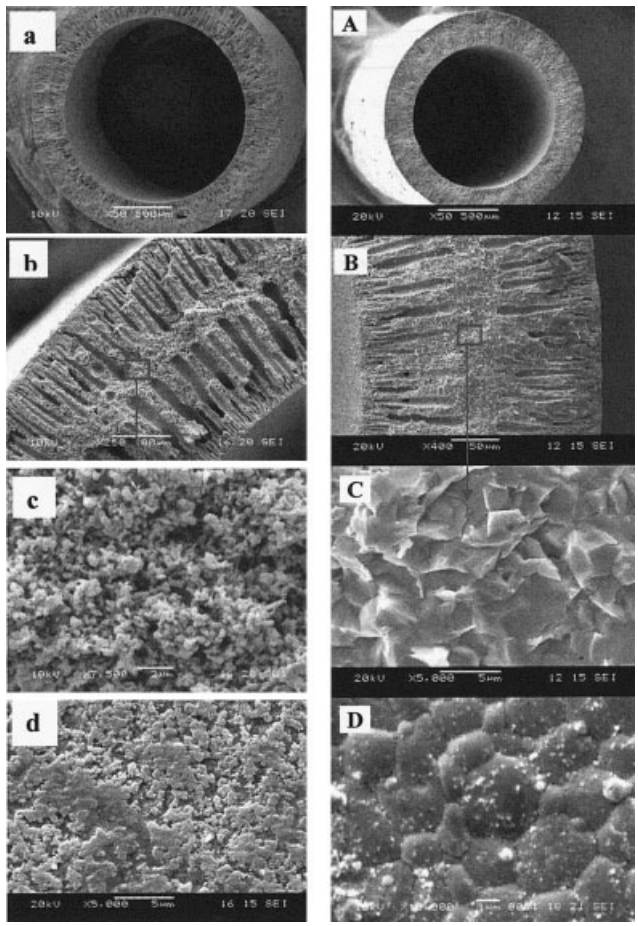

Figure 5. SEM microphotographs of the SCYb hollow-fiber membrane.

(a) Cross section of the hollow-fiber precursor; (b) wall of the hollow-fiber precursor; (c) central sponge layer of the hollow-fiber precursor; (d) outer surface of the hollow-fiber precursor; (A) cross section of the sintered fiber; (B) wall of the sintered fiber; (C) central layer of the sintered fiber; (D) outer surface of the sintered hollow fiber.

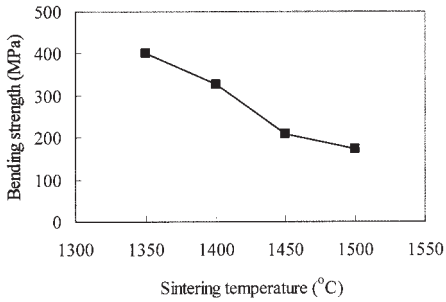

Figure 6. Mechanical strength of the SCYb hollow fibers sintered at different temperatures.

brane but also a possible leakage of joints of the system; the actual permeance value of the fiber should be lower than the above-calculated result. The gastightness of the membrane was also tested at high temperature during the hydrogen permeation experiments. It was further confirmed that the membrane is gastight because no nitrogen was detected at the feed compartment (hydrogen and argon) by gas chromatography at the operating temperature of 850°C.

The mechanical strength of the SCYb hollow-fiber membranes as a function of sintering temperature is shown in Figure 6. As can be seen, the mechanical strength of the hollow fibers decreases from 401 to 173 MPa as the sintering temperature is increased from 1350 to 1500°C. This is believed to be the result of grain growth as the sintering temperature increases.[12] However, the gas permeation tests indicate that the surface defects of the membrane would be eliminated only at temperatures between 1450 and 1500°C; that is, fibers became gastight and by a further increase of sintering temperature to 1550°C, the membrane once again becomes porous. We previously observed the same result.[6] Therefore, it is essential that sintering of SCYb hollow-fiber membranes should be carried out at 1450°C so that these fiber products possess both gastight property and sufficient mechanical strength.

Figure 7 shows the XRD patterns of the membrane material, of the fresh membrane, and of the used membranes, indicating that the fresh membrane remains in the perovskite structure as the SCYb powders after the phase inversion and sintering processes. After performing the hydrogen permeation experiments, a small amount of impurity phase identified as CeO_2 and

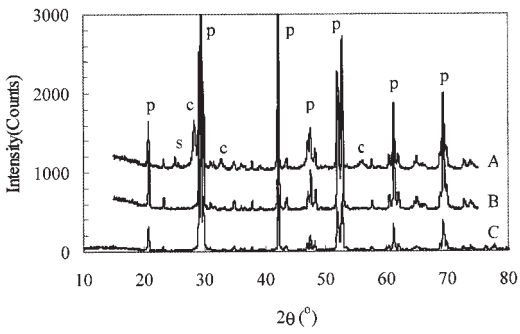

Figure 7. XRD patterns of the SCYb powders and hollow-fiber membranes.

(A) SCYb fiber after permeation (p, perovskite; c, CeO_2; s, $SrCO_3$); (B) SCYb fiber before permeation; (C) SCYb powder.

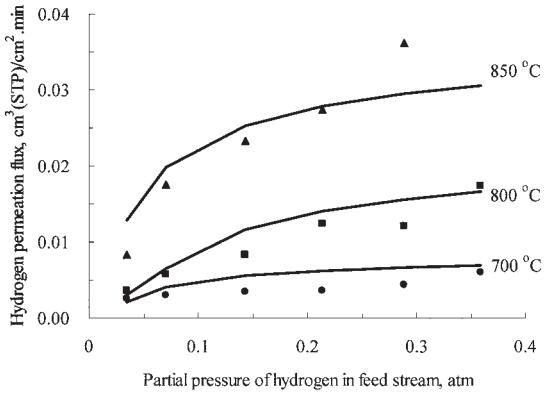

Figure 8. Effect of hydrogen partial pressure in the shell side on the hydrogen (proton) permeation flux at various temperatures.

p_{O_2} = 0.21 atm.

$SrCO_3$ occurred on the outer surface of the membrane, although primarily it still retains the perovskite structure. Moreover, the hydrogen permeation rate was not noticeably deteriorated after 2 weeks, which suggests that the SCYb membrane has a satisfactory stability.

Hydrogen permeation in the hollow-fiber membrane module

The proton conduction properties of the SCYb hollow-fiber membranes under different temperatures and feed concentrations are presented in terms of hydrogen permeation flux in the following section. The membrane characteristics and both diffusional and equilibrium parameters for calculation of theoretical hydrogen permeation in the membrane module are summarized in Table 2.

Figure 8 shows hydrogen permeation rates for the SCYb hollow-fiber membrane as a function of hydrogen partial pressure, which was obtained by adjusting the flow rates of hydrogen and argon gases while retaining a constant total gas flow rate, under different temperatures. The oxygen partial pressure in the opposite compartment was kept at 0.21 atm, that is, air was used as the oxygen source. It can be seen that the hydrogen permeation rate increases with increasing hydrogen partial pressure and also increases with increasing temperature. The experimental data, in general, are lower than the theoretical results presented by solid lines. The reason for this might be that the resistances of surface exchange reactions, which were ignored in the mathematical model, may have an effect on hydrogen permeation. Because the hollow fiber shows an asymmetric structure (that is, dense outer surface of the SCYb hollow fiber), there may be insufficient surface area provided in the outer surface, resulting in a substantially reduced surface exchange reaction rate. Therefore, more work should be carried out to increase the surface areas of both the inner and outer surfaces of the membrane. In addition, both the theoretical results and the experimental data indicate that the hydrogen permeation rate may be improved by increasing temperature rather than by increasing the hydrogen partial pressure in the feed.

Effects of oxygen partial pressure in the air stream side on the hydrogen permeation rate through the SCYb hollow-fiber

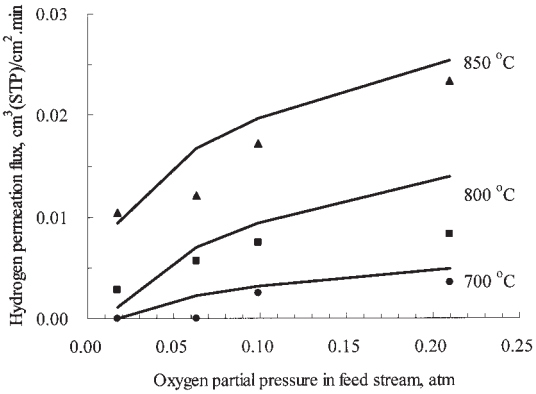

Figure 9. Effect of oxygen partial pressure in lumen side on the hydrogen (proton) permeation flux at various temperatures.

p_{H_2} = 0.142 atm.

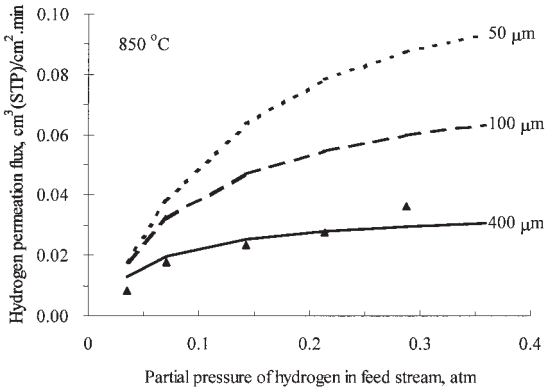

Figure 10. Hydrogen permeation flux under various membrane thicknesses.

T = 850°C, p_{O_2} = 0.21 atm.

membrane under different temperatures are shown in Figure 9, where the hydrogen partial pressure was maintained at a constant 0.142 atm. It can be seen that, as the oxygen partial pressure increases, more electron holes can be produced, resulting in an increase in the hole concentration on the membrane surface exposed to the air stream (Figure 2). Therefore, the permeation flux of charged defects or the hydrogen permeation rate is improved as a result of the increasing driving force, as reflected in Figure 9. However, at higher oxygen partial pressures, formation rate of the hole shows less effect in the defect permeation process, which suggests that the permeation process is controlled by other steps such as the formation rate of proton. As a result, the beneficial effect of further increasing oxygen concentration gradually diminishes. Again, in general, the experimental data are lower than the theoretical results as shown in solid lines. However, the general trends are sufficiently clear to merit a meaningful comparison between the experimental and theoretical results.

It should be mentioned that the membrane thickness used for the calculations is the difference between the outer and inner radius of the hollow fibers, that is, 400 μm. However, if the outer dense layer is taken as the actual membrane thickness for hydrogen permeation (that is, $<$50 μm), the theoretical results would be much higher than those of the experimental data as shown in Figure 10. For example, the hydrogen permeation flux for the membrane with thickness of 50 μm at 850°C may approach 0.08 cm^3 (STP) cm^{-2} min^{-1}, which is similar to the experimental results obtained by Hamakawa et al.,[4] whereas the actual permeation flux in the hollow-fiber membrane is only 0.02 cm^3 (STP) cm^{-2} min^{-1}. This suggests that both inner and outer surfaces of the membrane are dense. Also, densification of the middle section of the fiber further leads to the membrane having its thickness equivalent to the fiber wall thickness. It is envisaged that if both dense skin layers in the inner and outer membrane surfaces are eliminated, leaving the fingerlike pore structures on both the membrane surfaces for enhanced surface reactions and central dense layer for the selective permeation, the hydrogen permeation flux would be expected to be substantially increased.

Figure 11 provides a theoretical comparison of the cocurrent and countercurrent flow patterns where the flow permeation profiles of proton and oxygen vacancy at 850°C are plotted against the effective distance from the air feed entrance. As expected, the proton permeation rate decreases as the gases pass through the hollow-fiber membrane, whereas the permeation rate of oxygen vacancy increases. This phenomenon is explained by the fact that increasing amounts of water vapor are produced as the reactions proceeds, leading to the increase in vapor concentration in the oxygen stream. Although the difference in the permeation profile occurs between the cocurrent and the countercurrent flows, the total amount of hydrogen permeation is almost the same because the concentrations of both hydrogen and oxygen are high, and so they remain relatively unchanged because of the permeation and reaction.

Conclusions

$SrCe_{0.95}Yb_{0.05}O_{3-\alpha}$ (SCYb) hollow-fiber membranes with desirable length were successfully prepared by means of an immersion-induced phase-inversion/sintering technique. To sinter the SCYb hollow-fiber precursor into a dense membrane, a programmed sintering process should be adopted. The obvious hydrogen permeation (or proton conduction) through the resulting dense SCYb hollow-fiber membranes generally oc-

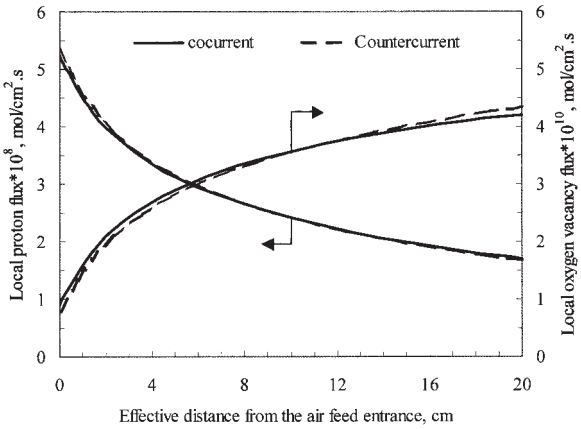

Figure 11. Comparison between the countercurrent and cocurrent flow operations.

T = 850°C, p_{H_2} = 0.2 atm, p_{O_2} = 0.21 atm.

curs after the applied temperature is >700°C. The hydrogen permeation flux increases with increasing hydrogen and oxygen concentrations, characterized by a nonlinear relationship. As the temperature increases to 850°C, the hydrogen permeation flux is noticeably increased. The surface exchange reactions may contribute some resistances to hydrogen permeation and thus should be taken into the account in a more rigorous mathematical model. However, because of the lack of reaction kinetic data, theoretical calculation with inclusion of surface exchange reactions at this stage is not possible. With both the length of fiber and the operating conditions used, the flow patterns show no noticeable effect on the total hydrogen permeation flux.

Acknowledgments

The authors gratefully acknowledge the research funding provided by EPSRC in the United Kingdom (Grant No. GR/S12203).

Notation

A_m = logarithm average membrane area, cm^2
C = concentration of defects or gas, mol cm^{-3}
D = effective diffusivity of defects, $cm^2\ s^{-1}$
J = molar flux of defects, mol $cm^{-2}\ s^{-1}$
K_1 = equilibrium constant for reaction 1, mol cm^{-3} $atm^{-0.5}$
K_2 = equilibrium constant for reaction 2, mol cm^{-3} atm^{-1}
K_3 = equilibrium constant for reaction 3, atm^{-1}
L = length of the reactor (hollow fiber), cm
n = number of hollow fibers
N = molar flow rate, mol s^{-1}
$p_{l,\ ps}$ = lumen or shell side pressure, atm
V_l, V_s = volumetric feed flow rate of air or hydrogen gas stream, $cm^3\ s^{-1}$ (STP)
R = ideal gas constant
$R_{o,\ Rin,\ Rm}$ = outer, inner, or log-mean radius of hollow fiber, cm
t = transport number of defects
T = operating temperature, K
y = molar fraction in gas stream
Yb_{Ce} = concentration of dopant, mol cm^{-3}
z = defect's charge number

Subscripts

h = hole
l = lumen side of the hollow fiber
p = proton
V = vacancy
s = shell side of the hollow fiber
I = hydrogen feed side
II = oxygen feed side

Literature Cited

1. Iwahara H. Oxide-ionic and protonic conductors based on perovskite-type oxides and their possible applications. *Solid State Ionics.* 1992; 52:99-104.
2. Iwahara H. Technological challenges in the application of proton conducting ceramics. *Solid State Ionics.* 1995;77:289-298.
3. Iwahara H, Esaka T, Uchida H, Maeda N. Proton conduction in sintered oxides and its application to steam electrolysis for hydrogen production. *Solid States Ionics.* 1981;3/4:359-363.
4. Hamakawa S, Li L, Li A, Iglesia E. Synthesis and hydrogen permeation properties of membranes based on dense $SrCe_{0.95}Yb_{0.05}O_{3-\alpha}$. *Solid State Ionics.* 2002;48:71-81.
5. Tan XY, Liu SM, Li K. Preparation and characterization of inorganic hollow fiber membranes. *J Membr Sci.* 2001;188:87-95.
6. Liu SM, Tan XY, Li K, Hughes R. Preparation and characterization of $SrCe_{0.95}Yb_{0.05}O_{2.975}$ hollow fiber membranes. *J Membr Sci.* 2001;193: 249-260.
7. Tan XY, Liu YT, Li K. Preparation of $La_{0.6}Sr_{0.4}Co_{0.2}Fe_{0.8}O_{3-\alpha}$ hollow fiber membranes for oxygen production by a phase-inversion/sintering technique. *Ind Eng Chem Res.* 2005;44:61-66.
8. Tan XY, Liu YT, Li K. Mixed conducting ceramic hollow fiber membranes for air separation. *AIChE J.* 2005:51:1991-2000.
9. Tan XY, Liu SM, Li K, Hughes R. Theoretical analysis of ion permeation through mixed conducting membranes and its application to dehydrogenation reactions. *Solid State Ionics.* 2000;138:149-159.
10. Slade RLT, Singh N. Systematic examination of hydrogen ion conduction in rare-earth doped barium cerate ceramics. *Solid State Ionics.* 1991;46:111-115.
11. Uchida H, Maeda N, Iwahara H. Relation between proton and hole conduction in $SrCeO_3$ based solid electrolytes under water-containing atmospheres at high temperatures. *Solid State Ionics.* 1983;11:117-124.
12. Liu YT, Li K. Preparation and characterization of $SrCe_{0.95}Yb_{0.05}O_{2.975}$ hollow fiber membranes: Study on sintering process. *J Membr Sci.* 2005;259:47-54.
13. Condon JB, Schober T. Modeling of point defect migration in proton conducting ceramics. *Solid State Ionics.* 1997;97:51-58.
14. Schober T, Friedrich J, Condon JB. Effective hydrogen diffusivity in $SrCe_{0.95}Yb_{0.05}O_{3-\alpha}$ and $SrZr_{0.95}Yb_{0.05}O_{3-\alpha}$. *Solid Sates Ionics.* 1995; 77:175-179.
15. Souza RAD, Kilner JA, Jeynes C. The application of secondary ion mass spectrometry (SIMS) to the study of high temperature proton conductors (HTPC). *Solid State Ionics.* 1997;97:409-419.
16. Uchida H, Yoshikawa H, Iwahara H. Dissolution of water vapor (or hydrogen) and proton conduction in $SrCeO_3$ based oxides at high temperatures. *Solid State Ionics.* 1989;35:229-234.
17. Guan J, Dorris SE, Balachandran U, Liu M. Transport properties of $BaCe_{0.95}Y_{0.05}O_{3-\alpha}$ and its application for hydrogen separation. *Solid State Ionics.* 1998;110:303-310.

Appendix A: Transfer Equations of Charged Defects in SCYb Membranes

In the following, the charged defects are defined using the Kröger–Vink notation: $O_O^{\times}$ stands for lattice oxygen, $V_O^{\cdot\cdot}$ for oxygen vacancy, e' for free electron, $H^{\cdot}$ for proton, and $h^{\cdot}$ for electron hole.

The transport fluxes of charged defects in mixed conductors at steady state under the electrochemical potential gradient can be expressed by[9]

$$J_i = -D_i C_i \left[\frac{1 - t_i}{C_i} \frac{dC_i}{dx} - \sum_{j \neq i} \frac{z_i}{z_j} \frac{t_j}{C_j} \frac{dC_j}{dx} \right] \tag{A1}$$

where D, C, z, and t are the diffusivity, concentration, charge number, and the transport number of defect i ($i = p, V, h$), respectively.

Without external current applied, the following equation must be satisfied at steady state:

$$\sum z_i J_i = 0 \tag{A2}$$

Meanwhile, local electric neutrality must be satisfied everywhere in the membrane, that is

$$[Yb'_{Ce}] = C_p + C_h + 2C_V \tag{A3}$$

where $[Yb_{Ce}]$ is the concentration of the dopant.

Obviously, the concentration profiles of the defects in the membrane at steady state may be described by a group of ordinary differential equations, rewritten in the matrix form as

$$\bar{A}\,\frac{d\bar{C}}{dx} = \bar{B} \tag{A4}$$

where

$$\bar{A} = \begin{bmatrix} 1 - t_V & -2t_p\dfrac{C_V}{C_p} & -2t_h\dfrac{C_V}{C_h} \\ -\dfrac{1}{2}t_V\dfrac{C_p}{C_V} & 1 - t_p & -t_h\dfrac{C_p}{C_h} \\ 2 & 1 & 1 \end{bmatrix} \qquad \bar{B} = \begin{bmatrix} -\dfrac{J_V}{D_V} \\ -\dfrac{J_p}{D_p} \\ 0 \end{bmatrix}$$

$$\bar{C} = \begin{bmatrix} C_V \\ C_p \\ C_h \end{bmatrix} \tag{A4a}$$

with the boundary conditions:

$$x = 0 \qquad \bar{C}_i = C_i(I) \qquad x = L \qquad \bar{C}_i = C_i(II) \tag{A5}$$

where *I* and *II* stand for the hydrogen side and the oxygen side, respectively.

The defect concentrations on the membrane surfaces may be given assuming that all the surface exchange reactions are in equilibrium, that is, the defect transfer process is the controlling step.

On the oxygen side,

$$V_O^{\bullet\bullet} + 0.5O_2 \Leftrightarrow O_O^{\times} + 2h^{\bullet} \qquad K_1 = \frac{[h^{\bullet}]^2}{[V_O^{\bullet\bullet}]p_{O_2}^{1/2}} \tag{A6}$$

$$O_O^{\times} + 2H^{\bullet} \Leftrightarrow H_2O + V_O^{\bullet\bullet} \qquad K_2 = \frac{[H^{\bullet}]^2}{[V_O^{\bullet\bullet}]p_{H_2O}} \tag{A7}$$

On the hydrogen side, in addition to Eq. A7, the following reaction occurs:

$$H_2 + 2h^{\bullet} \Leftrightarrow 2H^{\bullet} \qquad K_3 = \frac{[H^{\bullet}]^2}{[h^{\bullet}]^2 p_{H_2}} \tag{A8}$$

It is the linear combination of the following successive reactions:

$$H_2 \Leftrightarrow 2H^{\bullet} + 2e' \qquad K_4 = \frac{[H^{\bullet}]^2[e']^2}{p_{H_2}} \tag{A9}$$

$$h^{\bullet} + e' \Leftrightarrow \text{nil} \qquad K_e = [h^{\bullet}][e'] \tag{A10}$$

where K_i ($i = 1, 2, 3, 4$) represent the equilibrium constants for the surface reactions.

The above surface reactions are not independent because the H_2O, H_2, and O_2 partial pressures must satisfy the thermodynamics for the reaction

$$H_2 + 0.5O_2 \Leftrightarrow H_2O \qquad K_w = \frac{p_{H_2O}}{p_{H_2}p_{O_2}^{1/2}} \tag{A11}$$

It should be noted that the above reactions might involve many substeps such as adsorption, dissociation, recombination, and charge transfer.

As a result, the corresponding defect concentrations on the membrane surfaces are given by solving Eqs. A6–A8 and A3 as

$$C_p(I) = \frac{\sqrt{(1 + 1/\sqrt{K_3p_{H_2}})^2 + 8[Yb'_{Ce}]/K_2p_{H_2O}} - (1 + 1/\sqrt{K_3p_{H_2}})}{4/K_2p_{H_2O}} \tag{A12a}$$

$$C_V(I) = C_p(I)^2/K_2p_{H_2O} \tag{A12b}$$

$$C_h(I) = C_p(I)/\sqrt{K_3p_{H_2}} \tag{A12c}$$

and

$$C_V(II) = \frac{1}{16}\left[\sqrt{(\sqrt{K_1p_{O_2}^{1/2}} + \sqrt{K_2p_{H_2O}})^2 + 8[Yb'_{Ce}]} - (\sqrt{K_1p_{O_2}^{1/2}} + \sqrt{K_2p_{H_2O}})\right]^2 \tag{A13a}$$

$$C_h(II) = \sqrt{K_1p_{O_2}^{1/2}C_V(II)} \tag{A13b}$$

$$C_p(II) = \sqrt{K_2p_{H_2O}C_V(II)} \tag{A13c}$$

Manuscript received May 21, 2005, and revision received Sept. 29, 2005.